Vol. 04, Iss. 1 (2026) 10-28, DOI: 10.61552/JME.2026.01.002

JME

Journal of Materials and Engineering

www.jme.aspur.rs

Research article

Structures, Adhesion Strengths, and Corrosion Resistance of Undoped, Nitrogen-Doped, and Platinum/Ruthenium/Nitrogen-Co-Doped Diamond-Like Carbon Thin Films

Nay Win Khun[a,b,*], Erjia Liu[a]

[a]*School of Mechanical and Aerospace Engineering, Nanyang Technological University, 50 Nanyang Avenue, Singapore 639798, Singapore,*
[b]*Institute of Microelectronics and Optoelectronics, Faculty of Electronics and Information Technology, Warsaw University of Technology, Koszykowa 75, 00-662 Warszawa, Poland.*

Keywords:

DLC
Pt, Ru, and N doping
Structures
Adhesion strength
Corrosion

* Corresponding author:

Nay Win Khun
E-mail: khunnaywin@gmail.com

Received: 29 October 2024
Revised: 15 November 2024
Accepted: 17 January 2025

A B S T R A C T

Three different types of diamond-like carbon (DLC) thin films, namely, DLC, nitrogen-doped DLC (N-DLC), and platinum/ruthenium/nitrogen-co-doped DLC (PtRuN-DLC) nanocomposite, were deposited on p-type silicon (p-Si) substrates via DC magnetron sputtering deposition to comparatively study their structures, adhesion strengths, and corrosion resistance in a 1 M HCl solution. The N doping caused graphitization of the N-DLC thin film, as the PtRuN-DLC nanocomposite thin film had the highest graphitization among the films. The DLC thin film and PtRuN-DLC nanocomposite thin film had the lowest and highest adhesion strengths, respectively. The N-DLC thin film exhibited lower corrosion resistance in the HCl solution than the DLC one due to its degraded sp^3-bonded cross-linking structure, while the PtRuN-DLC nanocomposite thin film had the highest corrosion resistance in the same solution due to the combined effects of its increased electrical resistivity and the co-doping of electrochemically nobler Pt and Ru than the C matrix. The co-doping of Pt, Ru, and N had a strong influence on the structures, adhesion strengths, and corrosion resistance of DLC thin films.

1. INTRODUCTION

DLC thin films have favourable properties for electronic, optical, mechanical, tribological, electrochemical, and biomedical applications [1-4]. Excellent chemical inertness of DLC thin films allows them to apply in chemical environments [4]. However, the insulating property of DLC thin films make them impossible in electrochemical applications [5].

Nowadays, N-DLC thin films are interested in electrochemical applications after they have been successfully made conductive by N doping and proved as promising N-DLC thin film electrodes for heavy metal tracing in aqueous solutions [6-8]. It is found that N doping also improves the adhesion strength of N-DLC thin films by relaxing their residual stress [9,10]. However, there is still a problem encountered with N doping, which lowers the corrosion resistance of N-DLC thin films by degrading their sp^3-bonded cross-linking structures with the increased number of sp^2 sites and, thereby, results in their prompt anodic dissolution in corrosive media [9,10]. The degraded corrosion resistance of N-DLC thin films can affect their electrochemical performance, such as sensitivity, repeatability, and durability [6-8]. Therefore, it becomes important to improve the corrosion resistance of N-DLC thin films to be successfully applied in electrochemical sensor applications.

Khun et al. [11] reported that co-doping of Pt and Ru is a possible way to improve the corrosion resistance of N-DLC thin films because noble Pt and Ru have high corrosion resistance. But the co-doping effects of Pt, Ru, and N on the bonding structures and corrosion behavior of PtRuN-DLC nanocomposite thin films in comparison to those of DLC and N-DLC thin films have not been widely studied and reported in the literature yet.

DLC thin films always contain pores due to an unbalance between the kinetics of film-forming species and the mobility of surface adatoms during deposition [12]. The presence of pores in DLC thin films allows permeation of electrolytes to their underlying substrates to cause anodic dissolution of the substrates [12]. Combined with the poor adhesion strength of DLC thin films, an attack of electrochemically active species in permeated electrolytes to film/substrate interfaces can lead to easy delamination of the films [10]. Therefore, detecting pores and assessing their effects on the corrosion-protective performance of DLC thin films hold the keys to understand their corrosion-induced degradation mechanisms in aggressive media. Zeng et al. [12] recommended that electrochemical impedance spectroscopy (EIS) was a sensitive technique in detecting nanopores in DLC thin films. A comparative study on the corrosion-protective performance of DLC and N-DLC thin films and PtRuN-DLC nanocomposite thin film in a highly acidic HCl solution should be carried out to understand the co-doping effects of Pt, Ru, and N on their corrosion behaviour for their successful applications.

In this study, the bonding structures, surface roughness, and adhesion strengths of DLC and N-DLC thin films and PtRuN-DLC nanocomposite thin film were comparatively studied using X-ray photoelectron spectroscopy (XPS), micro-Raman spectroscopy, atomic force microscopy (AFM), and micro-scratch test. Their corrosion behavior in a 1 M HCl solution was investigated using EIS.

2. EXPERIMENTAL DETAILS

2.1 Sample preparation

DLC and N-DLC thin films and PtRuN-DLC nanocomposite thin film were deposited on p-Si (100) (0.001-0.0035 Ωcm) substrates using an unbalanced magnetron sputtering deposition system (Penta Vacuum system with four target configurations) (Figure 1). Prior to the film deposition, the native surface oxides and contaminants of the Si substrates were removed with Ar^+ plasma in a vacuum chamber at a negative substrate bias of 250 V and a pressure of 10 mTorr for 20 minutes. For all the film depositions, a 4-inch graphite target (99.99%) and a 4-inch $Pt_{50}Ru_{50}$ target (99.99%) were used. The detailed deposition process parameters used in this study are presented in Table 1.

Fig. 1. Photo of an unbalanced magnetron sputtering deposition system used in this study.

2.2 Characterization

The chemical compositions and bonding structures of the thin films were characterized using XPS with an X-ray source of a monochromatic Al K_α line (hυ = 1486.71 eV). A pass energy of 160 eV was applied for their survey scans, and a pass energy of 40 eV was used for detail scans of their C 1s, C 1s + Ru 3d, N 1s, O 1s, and Pt 4f. For the depth profiling, the calibrated etching rate with a silicon dioxide (SiO_2) film was about 3 nm/min.

The bonding structures of the thin films were investigated by micro-Raman spectroscopy (Renishaw RM1000) equipped with a He-Ne laser of 632 nm in a range of 800-2000 cm^{-1}. Five measurements on each sample were carried out to average Raman data.

Table 1. Deposition process parameters for DLC and N-DLC thin films and PtRuN-DLC nanocomposite thin film.

	DC power of C target (W)	DC power of $Pt_{50}Ru_{50}$ target	Ar gas flow rate (sccm)	N_2 gas flow rate (sccm)	Deposition pressure (mTorr)	Substrate bias (-V)	Substrate rotation (rpm)	Deposition time (min)
DLC	650	nil	50	nil	4	20	10	60
N-DLC	650	nil	50	10	4	20	10	60
PtRuN-DLC	650	30	50	10	4	20	10	60

The surface topographies of the thin films were studied using AFM (Digital Instrument, S-3000) with a tapping mode Si_3N_4 cantilever in a scan size of 1 μm × 1 μm. The average value of arithmetic mean roughness, R_a, was determined from five measurements per sample.

The adhesion strengths of the thin films were evaluated using a micro-scratch tester (Shimadzu SST-101) with a diamond stylus of 30 μm in radius that was dragged down onto the film surfaces under progressive loading at room temperature (RT~22–24 ˚C). The scan amplitude and frequency, scratch rate, and down speed were 50 μm, 30 Hz, 10 μm/s, and 2 μm/s, respectively. Five measurements on each sample were conducted to take an average critical load.

The corrosion-protective performance of the thin films in a 1 M HCl solution was investigated by EIS using an Autolab Type II potentiostat/galvanostat with a three-electrode cell. The backsides of the film-coated samples with a size of 2 cm × 2 cm were coated with a gold layer for a good electrical connection during the electrochemical measurements. They had an exposed area of 1 cm in diameter in a circular shape. A standard calomel reference electrode (SCE) (244 mV vs. SHE at 25 ˚C) and a platinum mesh counter electrode were used. Their Nyquist and Bold plots were acquired at their respective free corrosion potentials in a frequency range of 10^5 to 10^{-3} Hz with an AC excitation signal of 10 mV after immersion in the HCl solution for 60 min.

3. RESULTS AND DISCUSSION

Figure 2 shows the XPS survey scans of the N-DLC thin film and PtRuN-DLC nanocomposite thin film in comparison. There are three main peaks attributed to C, N, and O elements on the XPS survey scan of the N-DLC thin film with a step-like structure that is attributed to piling-up of the background produced by one peak over another peaks [13]. The co-doping of Pt and Ru gives rise to additional Pt and Ru-related peaks on the XPS survey scan of the PtRuN-DLC nanocomposite thin film. The background signal is related to the production of inelastically scattered electrons underneath the sample surface, which exhibit their lost kinetic energies upon arrival to the surface and, thus, their higher binding energies than their core level peak energies according to $E_{BE} = h\nu - E_K - \varphi$, where E_{BE} is the binding energy, h is the Plank's constant, ν is the frequency of the X-ray photon, E_K is the kinetic energy, and φ is the work function of the spectrometer [13]. The XPS survey scan of the PtRuN-DLC nanocomposite thin film has a higher background especially on the higher binding energy side compared to that of the N-DLC thin film, indicating the higher production of inelastically scattered electrons as a result of the presence of surface metal oxides [14]. Nevertheless, no observation of any other traceable elements on the XPS survey scans of both the N-DLC thin film and PtRuN-DLC nanocomposite thin film confirms that both the thin films do not have any contaminated chemical elements.

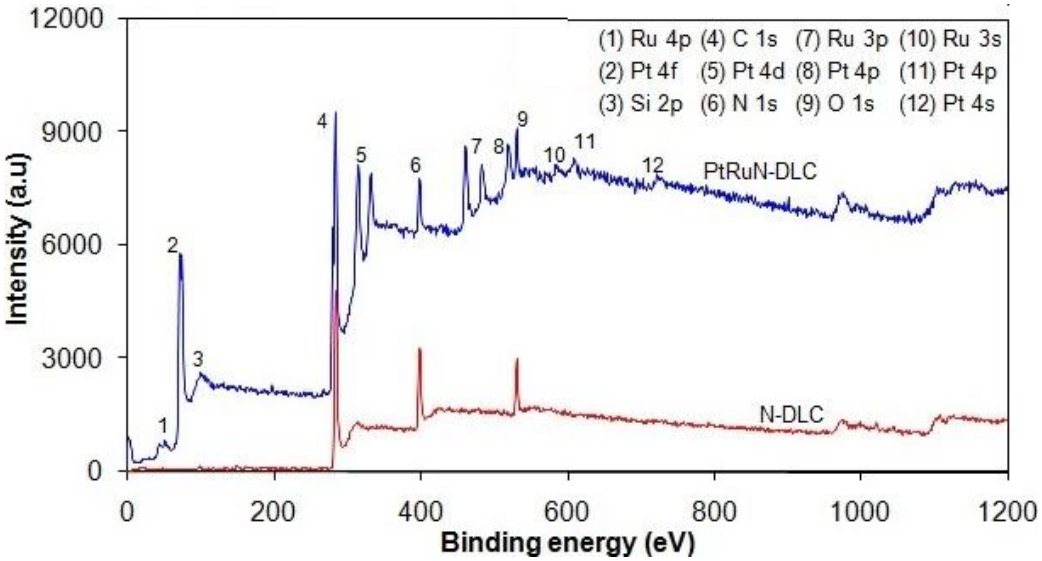

Fig. 2. XPS survey scans of N-DLC thin film and PtRuN-DLC nanocomposite thin film.

Figure 3a shows the depth profile of the DLC thin film in which its surface O content is about 12 at.% and its bulk O content at the etching time of 180 s is about 1.7 at.%. Its surface O is the result of exposure to the atmosphere after venting the deposition chamber, and its bulk O results from a reaction of sputtered C species with O species existing in the deposition chamber during the film deposition. An abrupt increase in its Si content at the etching time of about 6,400 s points out an interface between the film and Si substrate.

In Figure 3b, the N-DLC thin film has a surface O content of about 7.29 at.% and a bulk O content of 1.1 at.% at the etching time of 180 s, which both are lower than those of the DLC thin film. A great difference between the electronegativities of C (2.5) and O (3.5) causes a strong attraction between them to form C-O bonds, which is responsible for the O content [15]. When the N_2 gas is introduced into the deposition chamber, the N content reduces the C fraction and, thereby, the number of C-O bonds in the N-DLC thin film. A smaller difference between the electronegativities of N (3.0) and O (3.5) causes less attraction between them to form N-O bonds, so that the N doping cannot compensate for the decreased amount of C-O bonds, resulting in its lower surface and bulk O contents compared to those of the DLC thin film [15]. In addition, the introduction of N_2 gas during the film deposition probably reduces the concentration of O species in the deposition chamber as well as lessens interaction between C and O species.

The N content of the N-DLC thin film decreases from about 23.09 at.% to 8.89 at.% with etching from the surface to the bulk for 180 s. A fluctuation in the bulk N content of the N-DLC thin film in a range of 7.74–10.04 at.% is attributed to aggregation of N inclusions in it [16]. The interface between the N-DLC thin film and Si substrate is observed at a shorter etching time of about 4,800 s compared to that for the DLC thin film, indicating its lower film thickness. It was reported [17] that light nitrogen ions (14 amu) less effectively sputtered on the C target than heavy argon ions (40 amu) because the atomic mass of bombarding ions onto target atoms was important to the sputtering yield. In addition, ionization of N_2 gas is less efficient than that of Ar gas due to a strong bonding between two N atoms of a N_2 molecule [18,19]. Therefore, the introduction of N_2 gas during the film deposition under the same deposition pressure lowers the sputtering yield of the C target by reducing the fraction of Ar species in the deposition chamber, resulting in the lower thickness of the N-DLC thin film compared to that of the DLC thin film.

The PtRuN-DLC nanocomposite thin film has a lower surface O content of about 7.82 at.% and a lower bulk O content of about 0.99 at.% at the etching time of 180 s than the DLC thin film, confirming that the film deposition in the N_2 environment reduces the oxygen content. The surface O content of the PtRuN-DLC nanocomposite thin film is higher than that of the N-DLC thin film. The possible reason is that a difference between the electronegativities of Pt

(2.2) or Ru (2.2) and O is larger than that between C and O or N and O, resulting in more interaction between metals and O for the higher surface O content [15].

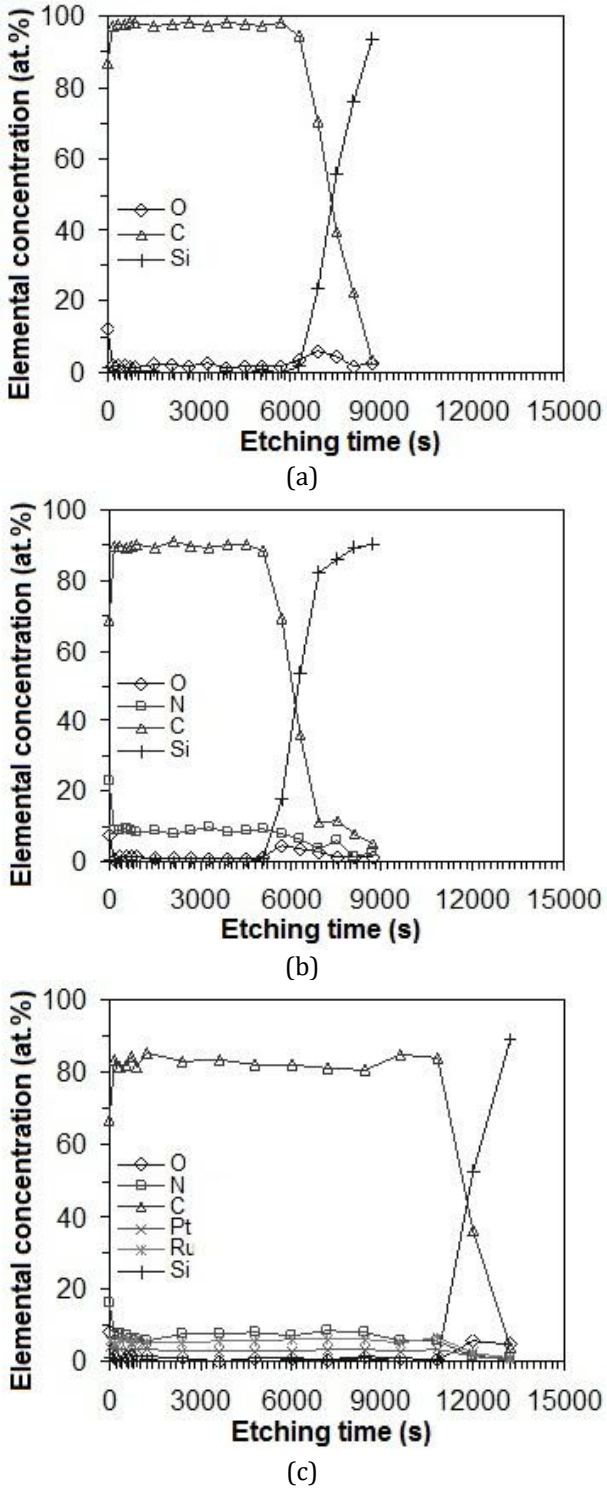

Fig. 3. Depth profiles of (a) DLC and (b) N-DLC thin films and (c) PtRuN-DLC nanocomposite thin film.

In Figure 3c, the surface N, Pt, and Ru contents of the PtRuN-DLC nanocomposite thin film are about 16.16 at.%, 3.62 at.%, and 5.73 at.%, respectively. After etching for 180 s, the N content apparently decreases to about 7.06 at.%, but the Pt and Ru contents remain almost unchanged. The bulk N content fluctuates in a range of 5.57–8.64 at.%, indicating the aggregation of N inclusions [16]. The abruptly increased Si content at the etching time of about 9,600 s is indicative of the film/substrate interface, as well as the highest thickness among the films used in this study. The PtRuN-DLC nanocomposite thin film deposition was carried out under the same deposition conditions used for the N-DLC thin film deposition, except for sputtering the $Pt_{50}Ru_{50}$ target. Therefore, the co-doping of Pt and Ru is responsible for the higher thickness of the PtRuN-DLC nanocomposite thin film than that of the N-DLC thin film. It is found that the Ru content is consistently higher than the Pt content throughout the thickness of the PtRuN-DLC nanocomposite thin film due to the PtRu core-shell structure [1,2,20].

In Figure 4a, the C 1s spectrum of the DLC thin film is composed of four peaks: the C-C sp^2 peak at about 284.1 eV, the C-C sp^3 peak at about 285 eV, the C-O peak at about 285.9 eV, and the C=O peak at about 287.7 eV [1,21]. The area ratio of its C-C sp^2 and C-C sp^3 peaks is 1.04.

The four peaks of C-C sp^2, C-C sp^3, C-O, and C-N bonds are found in the C 1s spectrum of the N-DLC thin film, as shown in Figure 4b. The C-N peak located at about 287.2 eV comes from the reaction between C and N species [7,21]. The N doping increases the area ratio of the C-C sp^2 and C-C sp^3 peaks of the N-DLC thin film to 1.25 as a result of the increased sp^2 sites in its C matrix because the N doping induces graphitization of its amorphous carbon structure [2,3,7,21]. Besides, the increased sp^2 sites in its amorphous carbon structure reduce its film density and, consequently, result in a relaxation of C-C sp^3 to C-C sp^2-bonding configuration [3,22].

In Figure 4c, the C 1s spectrum of the PtRuN-DLC nanocomposite thin film is overlapped entirely with Ru $3d_{3/2}$ and partially with Ru $3d_{5/2}$ [1,23]. Its C 1s + Ru 3d spectrum has two additional spin-orbit doublets of Ru^0 at about 280.6 eV and Ru-O at about 282.4 eV [1,11,23]. The PtRuN-DLC nanocomposite thin film has an area ratio of its C-C sp^2 and C-C sp^3 peaks of 1.48, which is

42.3% and 18.4% larger than those of the N-DLC and DLC thin films, respectively. It indicates that the co-doping of Pt, Ru, and N gives rise to the higher sp^2 content of the PtRuN-DLC nanocomposite thin film than the doping of N alone due to the combined effects of N and metal-induced graphitization of its amorphous carbon structure [1,2,11,24,25].

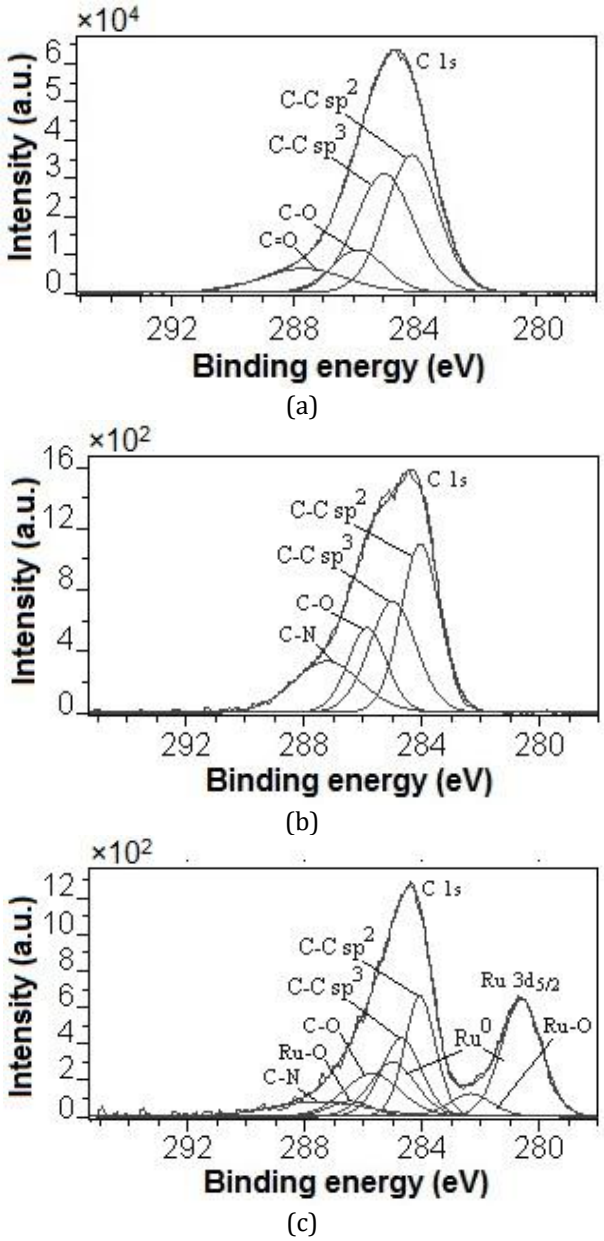

Fig. 4. Fitted XPS C 1s spectra of (a) DLC and (b) N-DLC thin films and (c) PtRuN-DLC nanocomposite thin film.

Figures 5a and 5b show the deconvoluted XPS N 1s spectra of the N-DLC thin film and PtRuN-DLC nanocomposite thin film, respectively, with the N-sp^2 peak at about 398.8 eV, the N-sp^3 peak at about 400.3 eV, and the N-O peak at about 401.2 eV [1,21]. The N-DLC thin film has an area ratio of its N-sp^2 and N-sp^3 peaks of 2.01, which is indicative of a preferential existence of N atoms in a sp^2-bonding configuration [1,21]. The PtRuN-DLC nanocomposite thin film has an area ratio of its N-sp^2 and N-sp^3 peaks of 2.8, which is 39.3% larger than that of the N-DLC thin film, indicating that the co-doping of Pt, Ru, and N results in a larger number of sp^2 bonds with N atoms than the doping of N alone by causing both N and metal-induced graphitization [1,2,11,24,25].

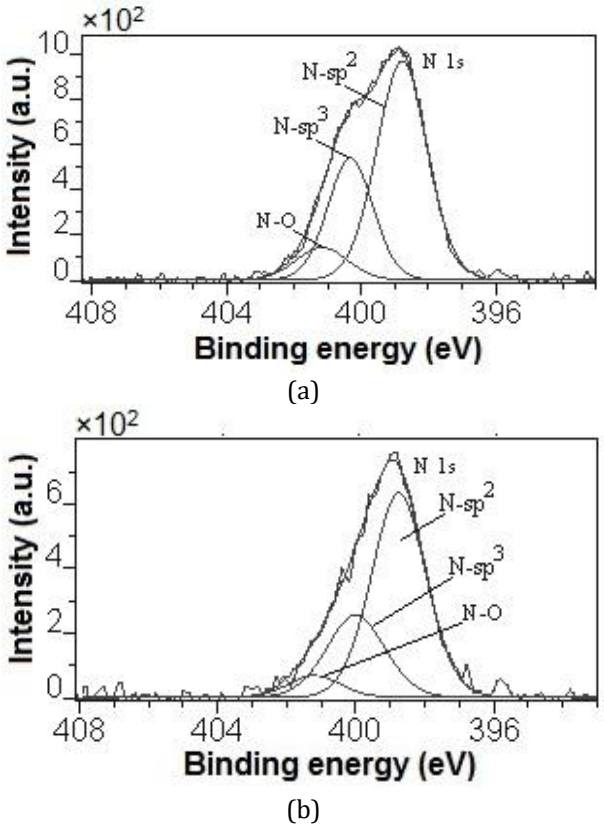

Fig. 5. Fitted XPS N 1s spectra of (a) N-DLC thin film and (b) PtRuN-DLC nanocomposite thin film.

Figure 6 shows the deconvoluted XPS Pt 4f spectrum of the PtRuN-DLC nanocomposite thin film with three spin-orbit doublets of Pt^0 at about 71.1 eV, Pt^{2+} at about 71.8 eV, and Pt^{4+} at about 73.5 eV resulting from neutral Pt and its different oxides, respectively [11]. The different oxidation states of Pt in the Pt 4f spectrum of the PtRuN-DLC nanocomposite thin film indicate a significant number of oxidized Pt species on its surface, which supports the claim that the presence of surface metal oxides causes the higher production of inelastically scattered electrons for its higher XPS background compared to that of the N-DLC thin film in Figure 2 [11].

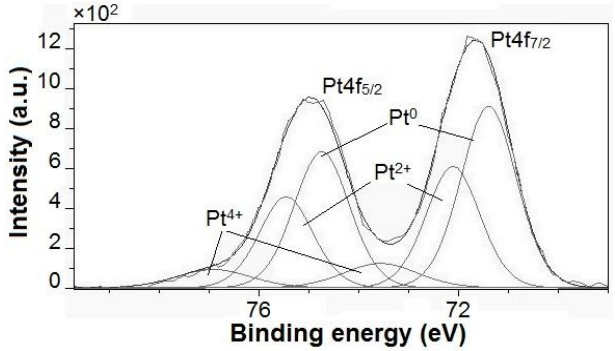

Fig. 6. Fitted XPS Pt 4f spectrum of PtRuN-DLC nanocomposite thin film.

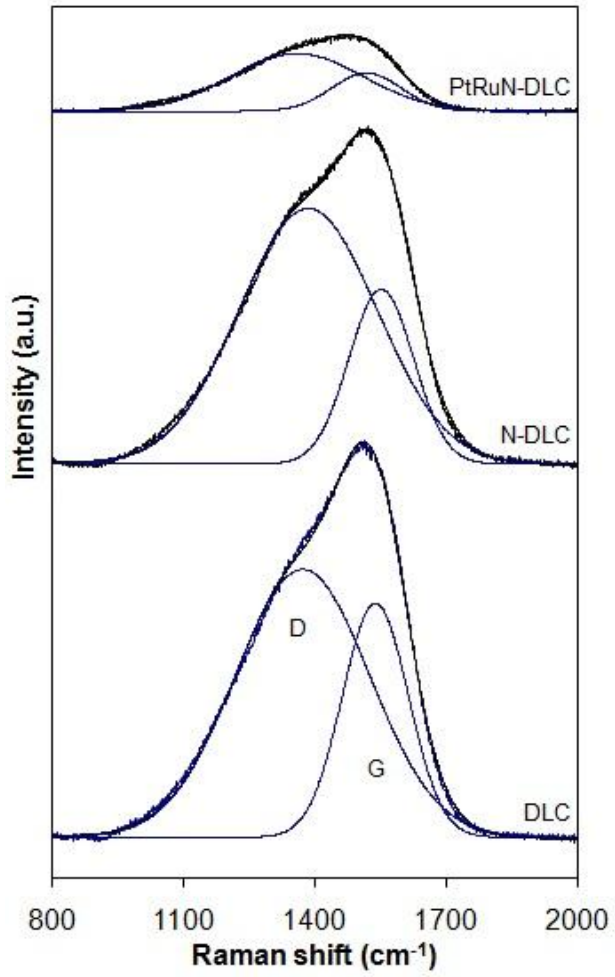

Fig. 7. Raman spectra of DLC and N-DLC thin films and PtRuN-DLC nanocomposite thin film.

In Figure 7, the Raman spectrum of the PtRuN-DLC nanocomposite thin film is apparently depressed compared to those of the DLC and N-DLC thin films because metal phases in its amorphous carbon structure are Raman inactive phases [2,3,11,26]. The Raman spectra of the DLC and N-DLC thin films and PtRuN-DLC nanocomposite thin film are fitted into G and D peaks using Gaussian functions with a linear background [27]. Since the D mode is the breathing vibration mode of all sp^2 sites only in rings, the D peak is mainly attributed to rings in an amorphous carbon structure [3,27]. As seen in Figure 7, the doping of N develops the D peak of the N-DLC thin film with respect to its G peak more than that of the DLC thin film, as the co-doping of Pt, Ru, and N results in the more apparent development of the D peak of the PtRuN-DLC nanocomposite thin film compared to those of both the DLC and N-DLC thin films. It indicates that the co-doping of Pt, Ru, and N gives rise to higher graphitization of the amorphous carbon structure than the doping of N alone.

In Figure 8a, the G and D peaks of the DLC thin film exist at about 1540 and 1373 cm^{-1}, respectively. The N doping shifts the G and D peaks of the N-DLC thin film to about 1552 cm^{-1} and 1385 cm^{-1} because the N doping increases sp^2 sites in its amorphous carbon structure via preferential π bonding of N atoms [3,21]. In addition, the upshifts of its G and D peak positions can be related to a decrease in the disorder of sp^2 bonds [28,29]. The PtRuN-DLC nanocomposite thin film has the G peak at about 1522 cm^{-1} and the D peak at about 1368 cm^{-1}, which both shift to lower wave numbers compared to those of the DLC and N-DLC thin films. The reason is that Pt and Ru have higher atomic masses than C, so the co-doping of heavier Pt and Ru increases the integrated atomic mass of the entire amorphous carbon structure, causing the downshifts of the G and D peaks [11,30,31].

In Figure 8b, the G and D peaks of the DLC thin film have full widths-at-half-maximum (FWHMs) of about 178 cm^{-1} and 359 cm^{-1}, respectively. The N-DLC thin film has a narrower $FWHM_G$ of about 174 cm^{-1} than the DLC film, confirming that the N doping decreases the disorder of sp^2 bonds since $FWHM_G$ is related to the disorder of sp^2 bonds [3,28]. Besides, its wider $FWHM_D$ of about 371 cm^{-1} implies an increase in the disorder of rings since a distribution of clusters with different ring orders broadens the D peak [21]. Doped N can adopt several bonding configurations, such as pyridine and pyrrole, in the amorphous carbon structure, so the N doping increases the number of non-sixfold rings and, consequently, the disorder of clusters [21,32].

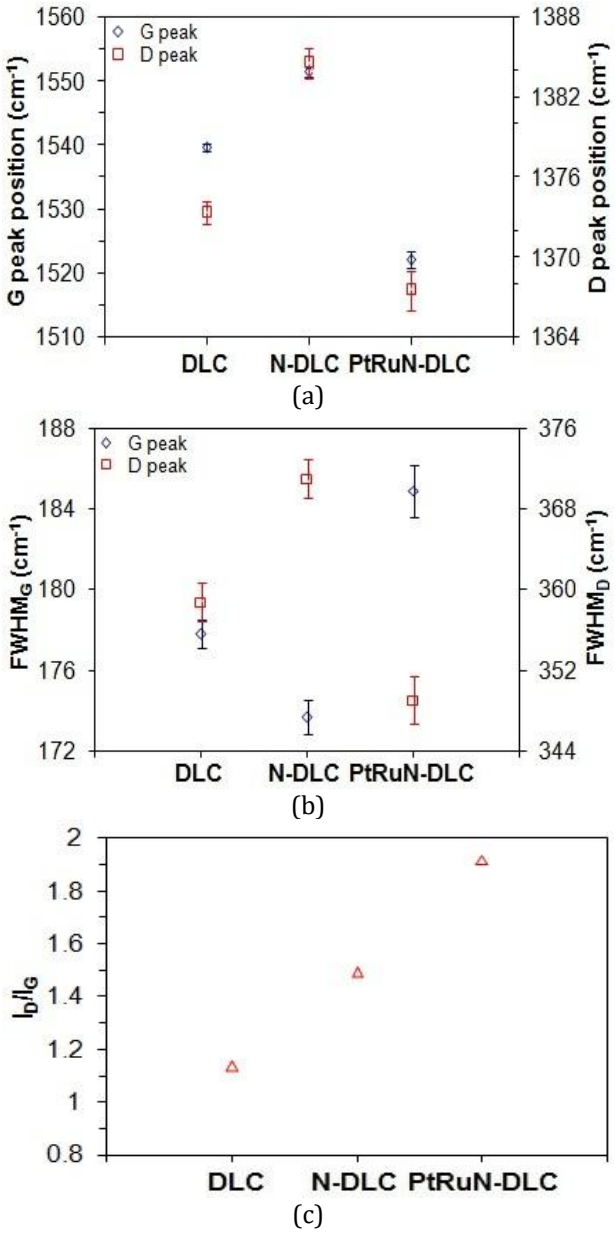

Fig. 8. (a) G and D peak positions, (b) $FWHM_G$ and $FWHM_D$, and (c) I_D/I_G of DLC and N-DLC thin films and PtRuN-DLC nanocomposite thin film.

The PtRuN-DLC nanocomposite thin film has the broadest $FWHM_G$ of about 185 cm^{-1}, as shown in Figure 8b, which is indicative of its highest disorder of sp^2 bonds among the films, probably due to the energetic bombardment of heavy Pt and Ru species onto the growing film during the film deposition [11,33]. However, its narrowest $FWHM_D$ of about 349 cm^{-1} indicates that the co-doping of Pt, Ru, and N gives rise to the lowest disorder of rings [20]. Amorphous carbon contacting with metal phases can graphitize at relatively low temperatures, and the sputtering process can provide sufficient energy to locally heat amorphous carbon on metal surfaces as a result of thermal spike [34,35]. Therefore, the resulting metal-induced graphitization of the PtRuN-DLC nanocomposite thin film lessens the disorder of rings by increasing the number of graphitic rings in its amorphous carbon structure in addition to the effect of its N-induced graphitization.

In Figure 8c, the intensity (I_D/I_G) ratio of the D and G peaks of the DLC thin film is 1.14. The N-DLC thin film has a larger I_D/I_G of 1.5, confirming that the N doping results in the graphitization of its amorphous carbon structure because the N doping encourages sp^2 sites to cluster [3,21,27]. The PtRuN-DLC nanocomposite thin film has the largest I_D/I_G of 1.92 due to the combined effects of N and metal-induced graphitization of its amorphous carbon structure [1,2,11,24,25].

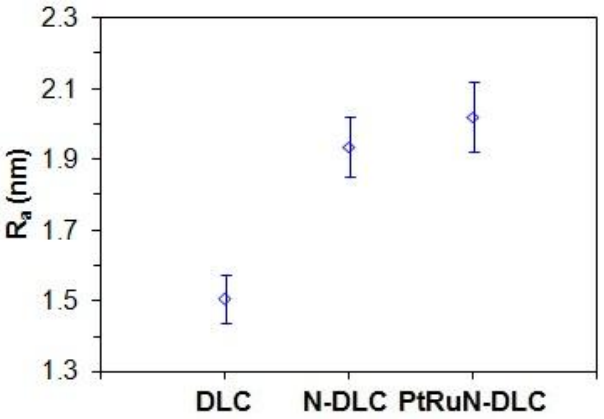

Fig. 9. R_a values of DLC and N-DLC thin films and PtRuN-DLC nanocomposite thin film.

In Figure 9, the R_a value of the DLC thin film is 1.5 nm, as the N-DLC thin film has a larger R_a value of 1.9 nm than the DLC thin film. The N doping prefers sp^2 bonding as well as encourages sp^2 sites to cluster [3,25]. Besides, N inclusions exist as aggregates in the amorphous carbon structure. Therefore, the resulting larger number of sp^2 sites reduces the density of the N-DLC thin film for its higher surface roughness, as the existence of N aggregates and graphitic phases roughens its surface [16,36,37]. The R_a value of the PtRuN-DLC nanocomposite thin film is 2 nm, which is the highest value among the films used in this study due to the combined effects of graphitization and aggregation associated with the co-doping of Pt, Ru, and N [2,11,36-38].

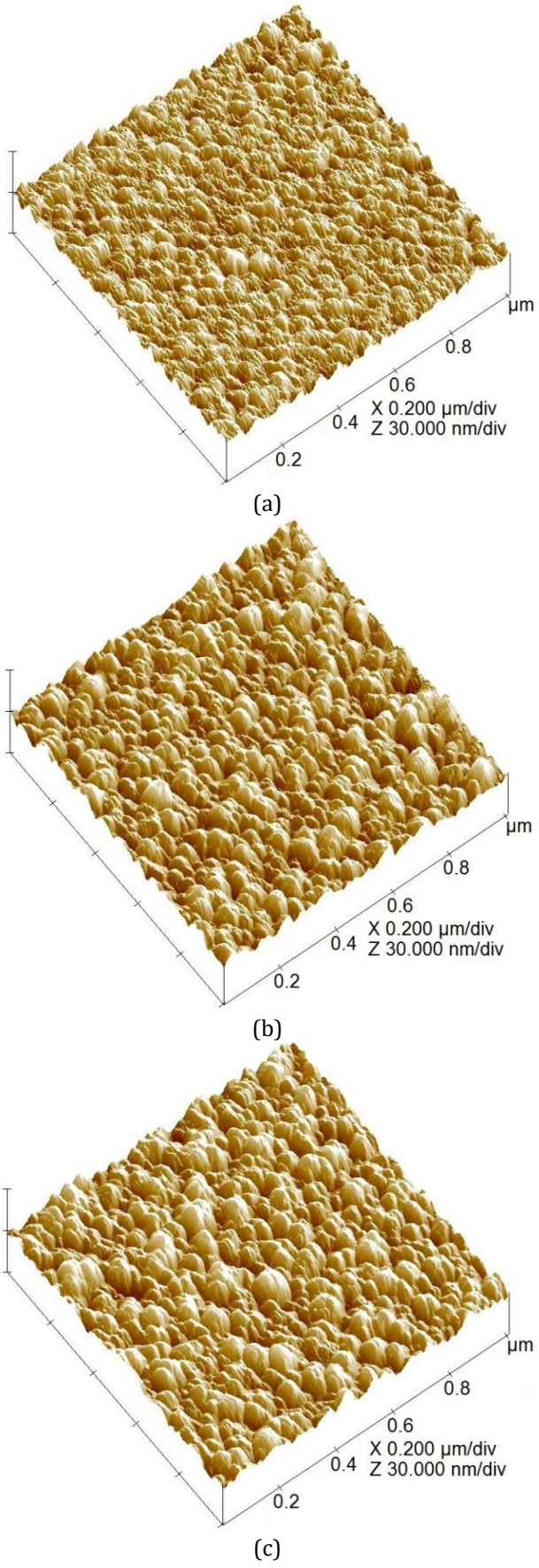

Fig. 10. AFM images showing surface topographies of (a) DLC and (b) N-DLC thin films and (c) PtRuN-DLC nanocomposite thin film.

Figures 10a, 10b, and 10c present the surface topographies of the DLC and N-DLC thin films and PtRuN-DLC nanocomposite thin film, respectively. In Figure 10a, the DLC thin film has round surface asperities, resulting from the distribution of sp^2-hybridized carbon clusters that lower its film density [16,39]. The surface asperities of the N-DLC thin film are larger than those of the DLC thin film, which results from the N-induced graphitization and N aggregation [2,3,16,36,37]. The PtRuN-DLC nanocomposite thin film has the largest surface asperities for its highest surface roughness among the films, which results from the combined effects of graphitization and aggregation induced by the co-doping of Pt, Ru, and N [2,3,11,16,36,37].

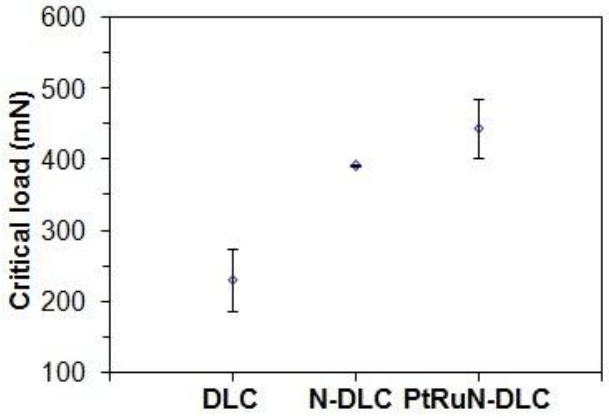

Fig. 11. Critical loads of DLC and N-DLC thin films and PtRuN-DLC nanocomposite thin film.

Figure 11 shows the critical loads of the DLC and N-DLC thin films and PtRuN-DLC nanocomposite thin film, which were taken from an abrupt change in tangential force during scratch testing [40]. The critical load of the DLC thin film is 232 mN. The N-DLC thin film has a 68.9% larger critical load of 392 mN than the DLC thin film, which is indicative of its higher adhesion strength. The residual stress in DLC thin film results from rigid sp^3-bonded cross-linking and bond distortion in its amorphous carbon structure caused by high energetic bombardment of sputtering species and, consequently, affects its adhesion to its underlying substrate [40,41]. Therefore, the larger number of sp^2 bonds in the N-DLC film can give rise to its higher adhesion strength because shorter sp^2 bonds reduce strain in the film compared to sp^3 bonds [30,36,37]. In addition, C=N bonds resulting from N doping also effectively reduce strain in the N-DLC film

since they have shorter bond lengths compared to those of either C-C or C=C bonds [36,42,43]. Because sp^2 bonds have a lower coordination number than sp^3 bonds, the increased number of sp^2 bonds in the N-DLC thin film associated with the N doping degrades its sp^3-bonded cross-linking structure [3,43]. At the same time, N aggregates and graphitic phases also degrade its sp^3-bonded cross-linking structure. These combined effects result in lower residual stress in the N-DLC thin film via its structural relaxation and, thereby, its higher adhesion strength. The PtRuN-DLC nanocomposite thin film has the highest critical load of 445 mN, which is 98.1% and 13.5% larger than those of the DLC and N-DLC thin films, respectively, as a result of its highest adhesion strength among the films. The metal-induced graphitization and metal aggregation associated with the co-doping of Pt, Ru, and N further relax residual stress in the PtRuN-DLC nanocomposite thin film and promote its adhesion strength in addition to the effects of N doping on its adhesion strength [2,11,44].

Figures 12a and 12b show the surface morphologies of the scratched DLC thin film observed at different magnifications. The DLC thin film has the lowest adhesion strength among the films. During the scratch testing, the diamond stylus continuously exerts interfacial shear stress between the film and substrate under progressive loading. When the stylus-induced interfacial shear stress exceeds the interfacial bond strength between the film and substrate, small interfacial cracks are abruptly initiated at the film/substrate interface and, then, propagated along the scratch trace thanks to the vibrational scanning motion of the diamond stylus under further progressive loading [45,46]. Thereafter, stress concentration occurring in front of the diamond stylus causes buckle-shaped delamination of the film along the scratch trace and, eventually, breaks it into small flakes via brittle fracture, as found in Figure 12b, when the stress concentration exceeds the cohesive strength of the film [45,46].

In Figures 12c and 12d, the N-DLC thin film does not exhibit any buckle-shaped delamination along the scratch trace, which is indicative of its higher adhesion strength. The higher adhesion strength of the N-DLC thin film results in a higher interfacial bond strength between the film and substrate than the cohesive strength of its underlying Si substrate, so that the removal of materials from the bulk region of the Si substrate as blocky-shaped fragments occurs at the critical load. No observation of any scratch-induced damage on the N-DLC thin film surface before the critical load implies that the N-DLC thin film has sufficient scratch resistance, although the N doping somehow degrades its sp^3-bonded cross-linking structure. It has been known that the N doping gives rise to the lower friction and wear of the N-DLC thin film compared to those of the DLC thin film [14,22]. The improved tribological performance of the N-DLC thin film also contributes to its higher resistance to scratch-induced damage. Since the thinner film has lower residual stress, the lower thickness of the N-DLC thin film than that of the DLC thin film is one of the reasons for its higher adhesion strength [47].

In Figure 12e, the PtRuN-DLC nanocomposite thin film exhibits surface damage only at its critical load, showing its relatively high scratch resistance. As shown in Figure 12f, the removal of film materials comes from the interfacial failure between the film and substrate, confirming the adhesive failure of the PtRuN-DLC nanocomposite thin film. Although the critical load of the PtRuN-DLC nanocomposite thin film is larger than that of the N-DLC thin film, the cohesive failure of its underlying Si substrate is not found in Figure 12f, probably due to its higher thickness that effectively lessens the transfer of stress concentration to the substrate [48].

Comparison of Figures 12a, 12c, and 12e shows that the scratch trace is apparently found on the surface of the PtRuN-DLC nanocomposite thin film as a result of its relatively low elastic recovery. Normally, elastic recovery of DLC is related to the average coordination of its amorphous carbon network [49]. The amorphous carbon network with a low coordination has less rigidity and, subsequently, a high tendency to have easy deformation during loading and low elastic recovery after unloading. Therefore, the co-doping of Pt, Ru, and N lowers the rigidity of the amorphous carbon network of the PtRuN-DLC nanocomposite thin film by increasing the number of sp^2 bonds via its N and metal-induced graphitization since the coordination number of sp^2 bonds is lower than that of sp^3 bonds [3]. The N

and metal aggregates and graphitic phases also lessen the rigidity of its amorphous carbon network by degrading its sp^3-bonded cross-linking structure. Therefore, its lower elastic recovery compared to those of the DLC and N-DLC thin films results in a more apparent scratch trace, left after the scratch testing, on its surface. Furthermore, the much lower elastic moduli of Pt and Ru compared to the carbon matrix are also responsible for its lower elastic recovery [50].

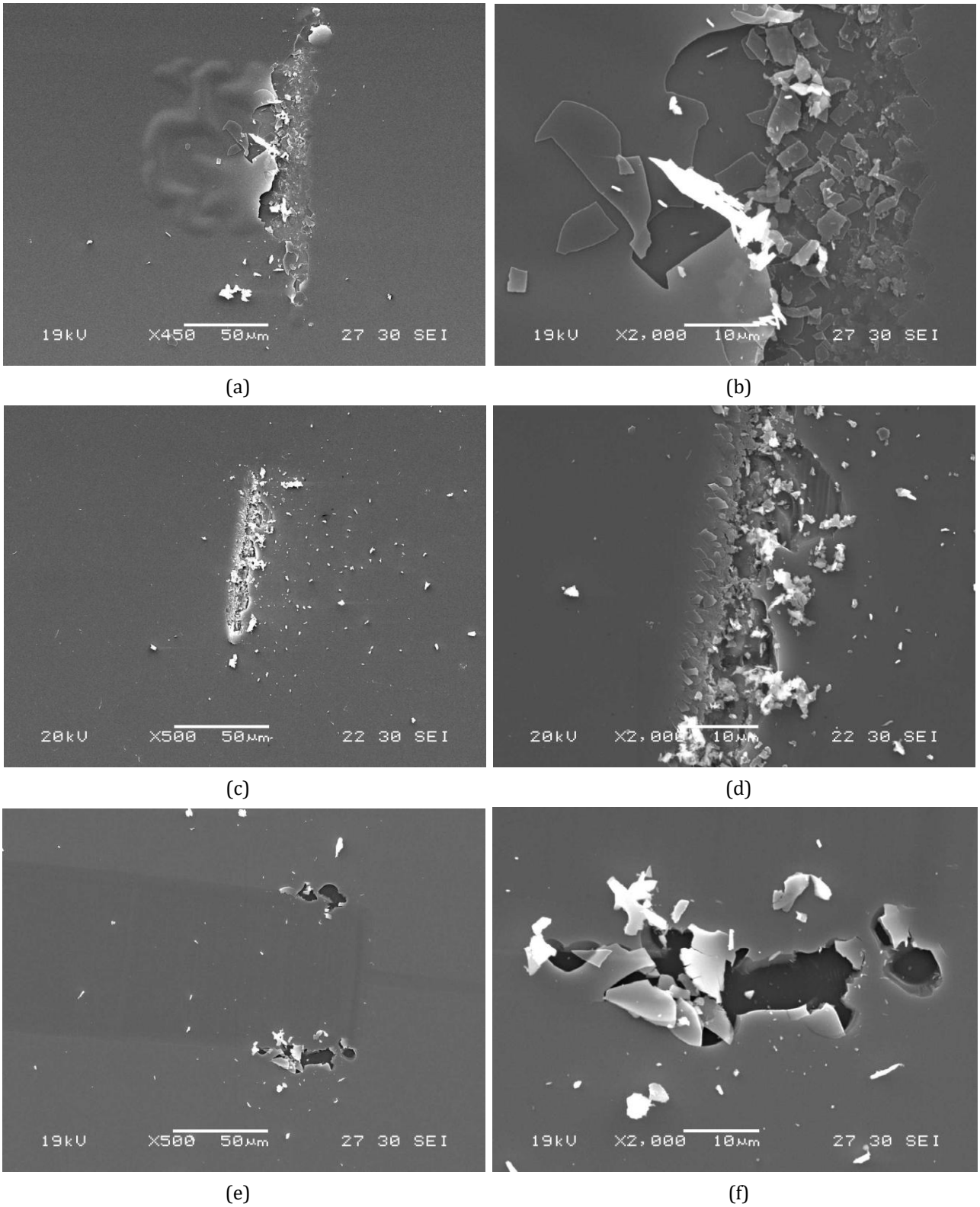

(a) (b)

(c) (d)

(e) (f)

Fig. 12. Surface morphologies of scratched (a and b) DLC and (c and d) N-DLC thin films and (e and f) PtRuN-DLC nanocomposite thin film observed at different magnifications.

It is supposed that the existence of PtRu aggregates on the surface of the PtRuN-DLC nanocomposite thin film can absorb stress concentration caused by the diamond stylus via their easy deformation at contact points, so that the film needs more scratch load to cause adhesive failure between the film and substrate. This could be one of the possible reasons for the higher critical load of the PtRuN-DLC nanocomposite thin film than those of the DLC and N-DLC thin films [50]. The highest thickness of the PtRuN-DLC nanocomposite thin film can also be related to its highest critical load because a thicker film requires a larger scratch load to transfer and exert stress on the film/substrate interface [48].

Table 2. Deposition process parameters used for N-DLC thin film and PtRuN-DLC nanocomposite thin film in Ref. [2].

	DC power of C target (W)	DC power of $Pt_{50}Ru_{50}$ target	Ar gas flow rate (sccm)	N_2 gas flow rate (sccm)	Deposition pressure (mTorr)	Substrate bias (-V)	Substrate rotation (rpm)	Deposition time (min)
N-DLC	850	nil	50	15	3	90	20	30
PtRuN-DLC	850	40	50	15	3	90	20	30

Table 2 presents the deposition process parameters used for the previous set of the N-DLC thin film and PtRuN-DLC nanocomposite thin film in Ref. [2]. Comparison of Table 1 and Table 2 shows that the lower deposition process parameters were used for the present set of the DLC and N-DLC thin films and PtRuN-DLC nanocomposite thin film but with the longer deposition time.

The present N-DLC thin film has a 11.5% higher N content than the previous one in Ref. [2], although the lower N_2 flow rate was used with the same Ar flow rate in this study. The possible reasons are that the higher deposition pressure used in this study allows the higher concentration of N species in the deposition chamber, while the significantly lower DC C-target power reduces the kinetic energies of impinging C species, which in turn promotes the formation of sp^2 bonds with more N atoms in the amorphous carbon structure since N atoms prefer π bonding [3,6,21]. In addition, the reduced kinetic energies of impinging C species may allow the incorporation of more N atoms in the film by giving a higher chance for reactions between C and N species.

The present PtRuN-DLC nanocomposite thin film has a 13.1% higher Pt content and a 16.9% higher Ru content than the previous one in Ref. [2]. Although the lower DC $Pt_{50}Ru_{50}$-target power was used in this study, the higher Pt and Ru contents of the present PtRuN-DLC nanocomposite thin film indicate that the significantly lower DC C-target power gives rise to the lower kinetic energies of impinging C species and, subsequently, allows the co-incorporation of more Pt and Ru atoms in the film. As a result, the higher Pt and Ru fractions in the present PtRuN-DLC nanocomposite thin film result in the lower fraction of its N content, which is confirmed by its 10.7% lower N content.

The present N-DLC thin film has a 15.4% larger I_D/I_G than the previous one in Ref. [2]. Since the higher kinetic energies of impinging C species can promote the number of sp^3 bonds in an amorphous carbon structure, their lower kinetic energies associated with the use of lower DC C-target power and negative substrate bias during the film deposition result in the higher sp^2 content of the N-DLC thin film [3]. The higher deposition pressure gives rise to the higher density of film-forming species in the deposition chamber and, consequently, their shorter mean free paths and lower kinetic energies, which also result in the higher sp^2 content of the N-DLC thin film [3]. As a result of encouraging sp^2 sites to cluster by N doping, the N-DLC thin film has a larger I_D/I_G than the DLC thin film. It is consistently found that the present PtRuN-DLC nanocomposite thin film also has a 20% larger I_D/I_G than the previous one in Ref. [2], although it has a slightly lower N content. Its higher Pt and Ru contents should also be taken into account in its larger I_D/I_G by correlating to its metal-induced graphitization [2,11,51]. The longer deposition time can generate a higher substrate temperature for higher graphitization of the amorphous carbon structure, which could contribute to the larger I_D/I_G of both the present N-DLC thin film and PtRuN-DLC nanocomposite thin film [52].

Both the present N-DLC thin film and PtRuN-DLC nanocomposite thin film have 134.6% and 69.5% larger R_a values than the previous ones in Ref. [2], respectively. The energetic bombardment of film-forming species compacts the film surface as well as forms the dense film by generating a high number of sp^3 bonds [53,54]. It can be seen that the lower kinetic energies of impinging C species associated with the lower DC C- and $Pt_{50}Ru_{50}$-target powers, lower negative substrate bias, and higher deposition pressure are responsible for their larger R_a values by means of their lower film densities associated with their higher sp^2 contents [53-55]. Besides, the higher number of graphitic phases contributes to the higher surface roughness of both the present N-DLC thin film and PtRuN-DLC nanocomposite thin film, as the higher Pt and Ru contents of the PtRuN-DLC nanocomposite thin film give an additional effect on its higher surface roughness by protruding more PtRu aggregates above its surface [11].

The present N-DLC thin film has a 9.2% larger critical load than the previous one in Ref. [2], as the present PtRuN-DLC nanocomposite thin film also has a 13.2% larger critical load compared to the previous one. The lower deposition process parameters used in this study result in their less sp^3-bonded cross-linking structures, and their resulting lower residual stresses lead to their improved adhesion strengths. The higher N content of the present N-DLC thin film also contributes to its higher adhesion strength. The lower N content of the present PtRuN-DLC nanocomposite thin film can affect its adhesion strength somehow, but its higher Pt and Ru contents are responsible for improving its adhesion strength via its metal-induced graphitization [1,2,11,24,25]. Comparison of the present and previous results clearly points out that the deposition parameters have significant influence on the structures, surface roughness, and adhesion strengths of both the N-DLC thin film and PtRuN-DLC nanocomposite thin film.

Figures 13a and 13b show the Nyquist and Bode plots of the DLC and N-DLC thin films and PtRuN-DLC nanocomposite thin film measured in a 1 M HCl solution, respectively. In Figure 13a, the semicircle of the N-DLC thin film has the smallest diameter among the films as well as a smaller diameter than that of the DLC thin film. This indicates that the N-DLC thin film has the lowest corrosion-protective performance in the HCl solution among the films, as its corrosion-protective performance is lower than that of the DLC thin film. Although both the DLC and N-DLC thin films have nearly complete semicircles, the semicircle of the PtRuN-DLC nanocomposite thin film is incomplete, which means that the PtRuN-DLC nanocomposite thin film has the highest corrosion-protective performance in the HCl solution. In Figure 13b, the PtRuN-DLC nanocomposite thin film exhibits the widest phase angles in an intermediate frequency range, confirming that it has the highest corrosion-protective performance in the HCl solution among the films [44,56].

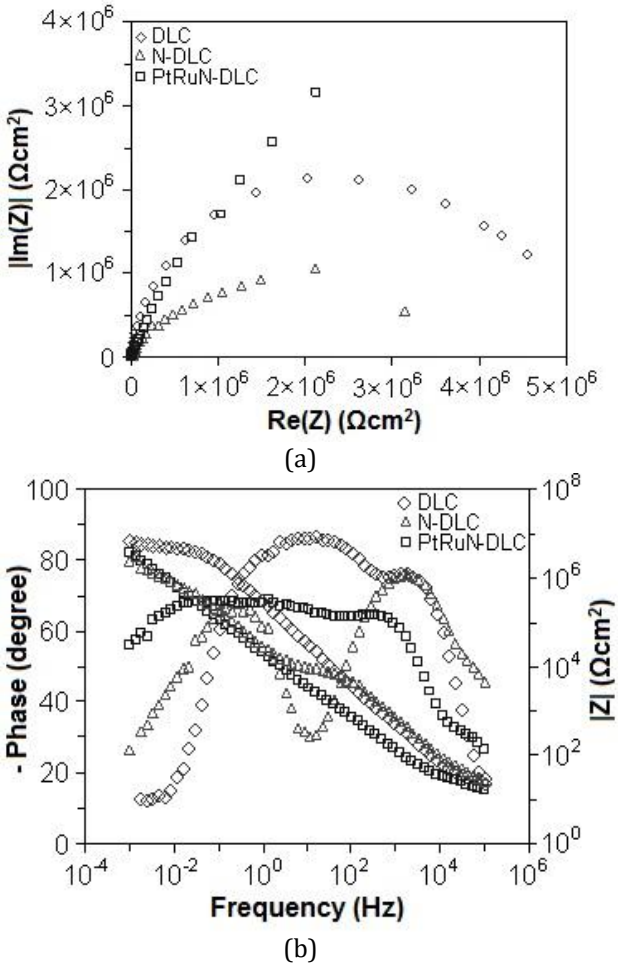

Fig. 13. (a) Nyquist and (c) Bode plots of DLC and N-DLC thin films and PtRuN-DLC nanocomposite thin film measured in a 1 M HCl solution.

An equivalent circuit model in Figure 14 was used to analyze the Nyquist and Bode plots in Figures 13a and 13b, respectively [44]. The replacement of capacitors in the circuit with constant-phase elements (Q) gave better curve-

fitting [48]. The EIS results are presented in Table 3. The equivalent circuit consists of the following elements: the resistance of the solution (R_1), the constant-phase element (Q_2) and charge transfer resistance (R_2) at the film/solution interface, and the constant-phase element (Q_3) and bulk resistance (R_3) of the film [44].

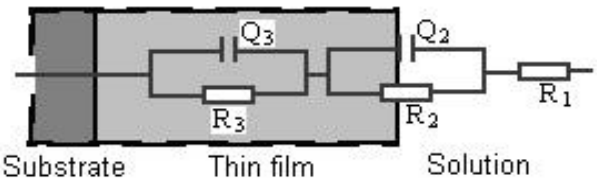

Fig. 14. An equivalent circuit used to fit the Nyquist and Bode plots in Figure 13.

Table 3. Fitted results from EIS spectra in Figures 13 using an equivalent circuit in Figure 14.

	R_1 (Ωcm^2)	R_2 (Ωcm^2)	Q_2 ($s^n/\Omega cm^2$)	n_2	R_3 (Ωcm^2)	Q_3 ($s^n/\Omega cm^2$)	n_3
DLC	19.33	2.12×10^6	0.201×10^{-6}	0.802	3.47×10^6	0.592×10^{-6}	0.984
N-DLC	10.14	6.94×10^3	0.176×10^{-6}	0.93	1.8×10^6	0.372×10^{-6}	0.787
PtRuN-DLC	10.66	10.09×10^6	0.702×10^{-6}	0.753	10.07×10^6	0.702×10^{-6}	0.753

In Table 3, the DLC thin film has a high R_2 value of 2.12×10^6 Ωcm^2, indicating its high charge transfer resistance in the highly acidic solution because the high content of sp^3 bonds in its amorphous carbon structure forms a rigid sp^3-bonded cross-linking network that prevents its prompt anodic dissolution [1,3,12,44]. The DLC film has a high R_3 value of 3.47×10^6 Ωcm^2. It is known that DLC thin film is always composed of various pores: open pores that allow permeation of the solution to the film/substrate interface and closed pores that do not allow permeation of the solution [12]. Pores develop with longer immersion via anodic dissolution of the film, so that the developed pores allow the solution to permeate to the underlying substrate, causing the electrolytic conduction in the bulk of the film [12]. Therefore, the high bulk resistivity of the DLC thin film points out its low porosity density to effectively hinder migration of electrolytic ions through the film to the Si substrate [12]. The observed CPEs in the equivalent circuit of the DLC thin film indicate a deviation from its ideal capacitive behavior, which may result from non-uniform current distribution induced by the non-uniform existence of sp^2 clusters in its amorphous carbon structure [57].

The N-DLC thin film has a significantly lower R_2 value of 6.94×10^3 Ωcm^2 than the DLC thin film, which can be correlated to its decreased corrosion resistance in the HCl solution with the N doping. This can be explained by its degraded sp^3-bonded cross-linking structure associated with N-induced structural imperfections such as changes in sp^2 and sp^3 contents, N aggregates, and graphitic phases [1,10,11,44]. In addition, the increased electrical conductivity of the N-DLC thin film accelerates corrosion reactions between the film and the solution, which is also responsible for its higher corrosion in the HCl solution compared to that of the insulating DLC thin film [1,10,11,44]. The N-DLC thin film has a lower R_3 value of 1.8×10^6 Ωcm^2 than the DLC thin film, as shown in Table 3, which is indicative of its lower bulk resistance. The N-induced structural degradation of the N-DLC thin film accelerates the development of pores via its prompt anodic dissolution in the HCl solution, which in turn allows communication between the electrolytic medium and substrate material through the migration of electrolytic ions [10-12,44]. The lower thickness of the N-DLC thin film than that of the DLC thin film gives rise to a shorter path as well as a higher porosity density for the faster and more permeation of the solution to communicate with its substrate, resulting in its higher electrolytic conduction [12]. At the same time, the improved electrical conductivity of the N-DLC thin film also contributes to its lower bulk resistance as a result of the higher kinetics of electron transfer through the film [10-12,44,58]. These combined effects lead to the lower bulk resistance of the N-DLC thin film.

In Table 3, the PtRuN-DLC nanocomposite thin film has the largest R_2 value of 10.09×10^6 Ωcm^2 among the films due to its highest charge transfer resistance in the HCl solution. Although the degradation of its sp^3-bonded cross-linking structure with the co-doping of Pt, Ru, and N should cause its highest corrosion in the HCl solution, its highest charge transfer resistance clearly points out that the co-doping of Pt and Ru is mainly responsible for its highest corrosion

resistance in the HCl solution because Pt and Ru are electrochemically nobler than the C matrix [11,59]. The PtRuN-DLC nanocomposite thin film has the largest R_3 value of 10.07×10^6, which is indicative of its highest bulk resistance. It was reported [55,56] that the distance between metal aggregates could drop to begin a conducting path in the bulk when the metal concentration reached a certain value. It is, therefore, supposed that the concentrations of Pt and Ru in the PtRuN-DLC nanocomposite thin film are not sufficient to make a conducting path in its bulk. Isolated metal aggregates are electrically inactive in the bulk of the film [60,61]. Schiffmann et al. [60] and Pleskov et al. [61] reported that the electrical conductivity of DLC thin film was associated with charge carrier hopping between sp^2-hybridized sites. It is hypothesized that the N doping probably promotes the charge carrier hopping effect by increasing sp^2 clusters in the film via its graphitization [12]. The distribution of embedded PtRu aggregates in the film degrades its electrical conductivity because they act as tunnel barriers between the nearest sp^2 clusters and prevent hopping conductance between them. Therefore, the co-doping of Pt and Ru gives rise to the highest electrical resistivity of the PtRuN-DLC nanocomposite thin film and, thereby, its highest charge transfer resistance in the HCl solution because the lowest kinetics of electron transfer through its bulk results in its slowest anodic dissolution [60-62]. Moreover, 3D distribution of PtRu aggregates in the film greatly drops the number of its open pores, effectively hinders the permeation of the solution, and, thereby, prevents its electrolytic conduction [11]. Furthermore, the highest thickness of the PtRuN-DLC nanocomposite thin film results in the lowest porosity density, since the thicker film makes the formation of open pores more difficult. Therefore, the highest electrical resistivity and lowest porosity density of the PtRuN-DLC nanocomposite thin film are responsible for its highest bulk resistance among the films.

The lowest n_2 and n_3 values (Table 3) of the PtRuN-DLC nanocomposite thin film indicate its largest deviation from the ideal double layer and bulk capacitive behavior, respectively. N aggregates and graphitic phases cause non-uniform electrochemical reaction rates on the surface of the PtRuN-DLC nanocomposite thin film because they have different sp^2 contents to cause localized changes in its electrical conductivity and, thereby, in its surface electrochemical reaction rates, while PtRu aggregates also contribute to the non-uniform electrochemical reaction rates on the film surface via their catalytic activities [44,63]. Besides, the highest surface roughness of the PtRuN-DLC nanocomposite thin film can result in the most uneven electron transfers over its surface for its most non-uniform electrochemical reaction rates [44,63]. Therefore, the above-mentioned effects are responsible for the lowest n_2 value of the PtRuN-DLC nanocomposite thin film. The lowest n_3 value of the PtRuN-DLC nanocomposite thin film is attributed to the non-uniform distribution of N and PtRu aggregates and graphitic phases within its bulk [62].

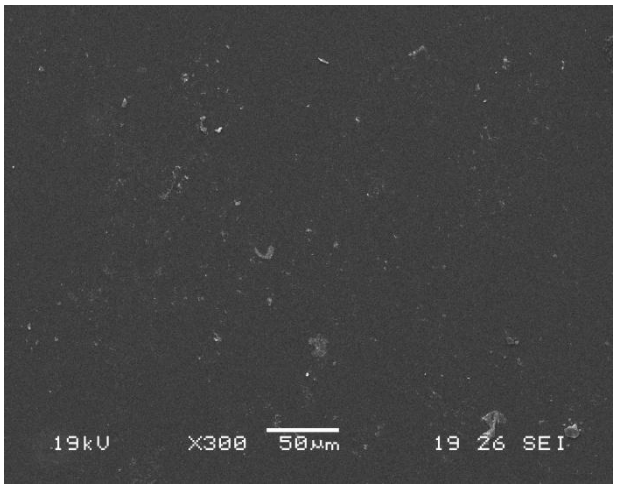

Fig. 15. Surface morphology of N-DLC thin film observed after EIS measurement in a 1 M HCl solution.

The corrosion-induced surface damage of the N-DLC thin film with the lowest corrosion resistance in the HCl solution was evaluated using SEM. Figure 15 shows the surface morphology of the N-DLC thin film tested in the HCl solution, from which its apparent surface damage caused by its anodic dissolution is not found, although it has the lowest corrosion resistance among the films. Distribution of corrosion products, which result from electrochemical reactions between the film and the solution, is apparently found on the N-DLC thin film surface, indicating its uniform corrosion in the HCl solution [10]. The SEM observation reveals that the N-DLC thin film has relatively high resistance to anodic dissolution in the highly acidic HCl solution.

4. CONCLUSION

The DLC and N-DLC thin films and PtRuN-DLC nanocomposite thin film were deposited on Si substrates to comparatively investigate their structures, surface roughness, adhesion strengths, and corrosion resistance in the 1 M HCl solution.

- The N-DLC thin film had a higher sp^2 content than the DLC thin film as a result of the N-induced graphitization, as the PtRuN-DLC nanocomposite thin film had the highest sp^2 content among the films due to the combined effects of N and metal-induced graphitization.
- The PtRuN-DLC nanocomposite thin film had the highest surface roughness resulting from N and metal aggregation and graphitic phases, as the N-DLC thin film had the higher surface roughness than the DLC thin film as a result of its graphitization.
- The N-DLC thin film had a higher critical load than the DLC thin film, which indicated its higher adhesion strength. The co-doping of Pt, Ru, and N gave rise to the highest critical load of the PtRuN-DLC nanocomposite thin film, which could be related to its highest adhesion strength.
- The N-DLC thin film had lower charger transfer and bulk resistance in the HCl solution than the DLC thin film due to its degraded sp^3-bonded cross-linking structure and promoted electrical conductivity. However, the co-doping of Pt, Ru, and N in the PtRuN-DLC nanocomposite thin film resulted in its highest charge transfer and bulk resistance in the same solution because Pt and Ru were electrochemically nobler than the C matrix. Besides, the distribution of PtRu aggregates degraded the electrical conductivity of the PtRuN-DLC nanocomposite thin film as well as decreased its porosity density to hinder the permeation of the solution through its bulk, resulting in its highest corrosion resistance in the HCl solution.
- The deposition process parameters, such as sputtering DC power, negative substrate bias, reactive gas flow rate, and deposition pressure, apparently affected the structures, surface roughness, and adhesion strengths of the N-DLC thin film and PtRuN-DLC nanocomposite thin film.

Acknowledgement

This work was supported by the research grant (EWI-0601-IRIS-035-00) from the Environment & Water Industry Development Council (EWI), Singapore.

REFERENCES

[1] N. W. Khun and E. Liu, "Structures, wettability, and corrosion resistance of annealed platinum/ruthenium/nitrogen-co-doped diamond-like carbon nanocomposite thin films at different temperatures," *Journal of Materials and Engineering*, vol. 3, iss. 2, pp. 217-229, 2025, doi: 10.61552/JME.2025.02.008.

[2] N. W. Khun and E. Liu, "Friction and wear of nitrogen-doped DLC coating and platinum/ruthenium/nitrogen-co-doped DLC nanocomposite coatings," *Journal of Materials and Engineering*, vol. 3, iss. 1, pp. 67–77, 2025, doi: 10.61552/JME.2025.01.004.

[3] J. Robertson, "Diamond-like carbon amorphous," *Materials Science and Engineering: R: Reports*, vol. 37, iss. 4–6, pp. 129–281, May 2002. doi: 10.1016/S0927-796X(02)00005-0.

[4] R. Shah, N. Pai, R. Khandekar, R. Aslam, Q. Wang, Z. Yan, and A. Rasenkranz, "DLC coatings in biomedical applications: review on current advantages, existing challenges, and future directions," *Surface and Coatings Technology*, vol. 487, pp. 131006, Jul. 2024, doi: 10.1016/j.surfcoat.2024.131006.

[5] J. Robertson, "Hard amorphous (diamond-like) carbons," *Progress in Solid State Chemistry*, vol. 21, iss. 4, pp. 199-333, 1991, doi: 10.1016/0079-6786(91)90002-H.

[6] N. W. Khun and E. Liu, "Linear sweep anodic stripping voltammetry of heavy metals from nitrogen-doped tetrahedral amorphous carbon thin films," *Electrochimica Acta*, vol. 54, iss. 10, pp. 2890-2898, Apr. 2009, doi: 10.1016/j.electacta.2008.11.014.

[7] L. X. Liu and E. Liu, "Nitrogenated diamond-like carbon films for metal tracing," *Surface and Coatings Technology*, vol. 198, iss. 1-3, pp. 189-193, Aug. 2005, doi: 10.1016/j.surfcoat.2004.10.031.

[8] A. Zeng, E. Liu, S. N. Tan, S. Zhang, and J. Gao, "Stripping voltammetric analysis of heavy metals at nitrogen-doped diamond-like film electrodes," *Electroanalysis*, vol. 14, iss. 18, pp. 1294-1298, Oct. 2002, doi: 10.1002/1521-4109(200210)14:18%3C1294::AID-ELAN1294%3E3.0.CO;2-R.

[9] L. S. Almeida, A. R. M. Souza, L. H. Costa, E. C. Rangel, M. D. Manfrinato, and L. S. Rossino, "Effect of nitrogen in the properties of diamond-like carbon coating on Ti6Al4V substrate," *Materials Research Express*, vol. 7, no. 6, pp. 065601, Jun. 2020, doi: 10.1088/2053-1591/ab94fb.

[10] N. W. Khun, E. Liu, and X. T. Zeng, "Corrosion behaviour of nitrogen-doped diamond-like carbon thin films in NaCl solutions," *Corrosion Science*, vol. 51, iss. 9, pp. 2158–2164, Sep. 2009. doi: 10.1016/j.corsci.2009.05.050.

[11] N. W. Khun, E. Liu, G. C. Yang, W. G. Ma, and S. P. Jiang, Structure and corrosion behaviour of platinum/ruthenium/nitrogen-doped diamond-like carbon thin films, *Journal of Applied Physics*, vol. 106, iss. 1, pp. 013506, July 2009. doi: 10.1063/1.3154022.

[12] A. Zeng, E. Liu, I.F. Annergren, S.N. Tan, S. Zhang, P. Hing, and J. Gao, "EIS capacitance diagnosis of nanoporosity effect on the corrosion protection of DLC films," *Diamond and Related Materials*, vol. 11, iss. 2, pp. 160-168, Feb. 2002, doi: 10.1016/S0925-9635(01)00568-4.

[13] D. N. G. Krishna and J. Philip, "Review on surface-characterization applications of X-ray photoelectron spectroscopy (XPS): recent developments and challenges," *Applied Surface Science Advances*, vol. 12, pp. 100332, Dec. 2022, doi: 10.1016/j.apsadv.2022.100332.

[14] J. Petrou, S. Diplas, H. Chiriac, and E. Hristoforou, "Magnetic and structural characterization of Fe-Ni films for high precision field sensing," *Journal of Optoelectronics and Advanced Materials*, vol. 8, no. 5, pp. 1715-1719, Oct. 2006.

[15] K. W. Frese Jr, "Calculation of surface binding energy for hydrogen, oxygen, and carbon atoms on metallic surfaces," *Surface Science*, vol. 182, iss. 1-2, pp. 85-97, Mar. 1987, doi: 10.1016/0039-6028(87)90090-2.

[16] E. Liu, X. Shi, H. S. Tan, L. K. Cheah, Z. Sun, B. K. Tay, and J. R. Shi, "The effect of nitrogen on the mechanical properties of tetrahedral amorphous carbon films deposited with a filtered cathodic vacuum arc," *Surface and Coatings Technology*, vol. 120-121, pp. 601-606, Nov. 1999, doi:10.1016/S0257-8972(99)00442-9.

[17] D. M. Mattox, "Handbook of physical vapour deposition (PVD) processing," Noyes Publications, 1998, USA.

[18] J. Liu, F. Sun, and H. Yu, "Enhancement of the molecular nitrogen dissociation and ionization levels by argon mixture in flue nitrogen plasma," *Current Applied Physics*, vol. 5, iss. 6, pp. 625-628, Sep. 2005, doi: 10.1016/j.cap.2004.08.009.

[19] J. L. Jauberteau, D. Duchesne, C. Girault, J. Aubreton, and A. Catherinot, "Spectroscopic study of a D.C. discharge in an argon-silane-nitrogen gas mixture under silicon nitride thin film deposition conditions," *Plasma Chemistry and Plasma Processing*, vol. 10, pp. 589-607, Dec. 1990, doi: 10.1007/BF01447266.

[20] P. K. Babu, H. S. Kim, E. Oldfield, and A. Wieckowski, "Electronic alternations caused by ruthenium in Pt-Ru alloy nanoparticles as revealed by electrochemical NMR," *The Journal of Physical Chemistry B*, vol. 107, iss. 31, pp. 7595-7600, Jul. 2008, doi: 10.1021/jp022679u.

[21] S. E. Rodil and S. Muhl, "Bonding in amorphous carbon nitride," *Diamond and Related Materials*, vol. 13, iss. 4-8, pp. 1521-1531, Aug. 2004, doi: 10.1016/j.diamond.2003.11.008.

[22] E. Liu, L. Li, B. Blanpain, and J. P. Cells, "Residual stresses of diamond and diamond-like carbon films," *Journal of Applied Physics*, vol. 98, pp. 073515, Oct. 2005, doi: 10.1063/1.2071451.

[23] R. K. Raman, A. K. Shukla, A. Gayen, M. S. Hegde, K. R. Priolkar, P. R. Sarode, and S. Emura, "Tailoring a Pt-Ru catalyst for enhanced methanol electro-oxidation," *Journal of Power Sources*, vol. 157, iss. 1, pp. 45-55, Jun. 2006, doi: 10.1016/j.jpowsour.2005.06.031.

[24] K. Bewiloguo, R. Wittorf, H. Thomsen, and M. Weber, "DLC-based coatings prepared by reactive d.c. magentron sputtering," *Thin Solid Films*, vol. 447-448, pp. 142-147, Jan. 2004, doi: 10.1016/S0040-6090(03)01088-5.

[25] A. F. Yetim, H. Kovaci, A. E. Kasapagul, Y. B. Bozkurt and A. Celik, "Influences of Ti, Al, and V metal doping on the structural, mechanical, and tribological properties of DLC films," *Diamond and Related Materials*, vol. 120, pp. 108639, Dec. 2021, doi: 10.1016/j.diamond.2021.108639.

[26] A. Y. Wang, K. R. Lee, J. P. Ahn, and J. H. Han, "Structure and mechanical properties of W incorporated diamond-like carbon films prepared by a hybrid ion beam deposition technique," *Carbon*, vol. 44, iss. 9, pp. 1826-1832, Aug. 2006, doi: 10.1016/j.carbon.2005.12.045.

[27] A. C. Ferrai and J. Robertson, "Interpretation of Raman spectra of disordered and amorphous carbon," *Physical Review B*, vol. 61, iss. 20, pp. 14095, May 2000, doi: 10.1103/PhysRevB.61.14095.

[28] D. Beeman, J. Silverman, R. Lynds, and M.R. Anderson, "Modeling studies of amorphous carbon," *Physical Review B*, vol. 30, iss. 2, pp. 870–875, 1984, doi: 10.1103/PhysRevB.30.870.

[29] H. L. Bai and E. Y. Jiang, "Improvement of the thermal stability of amorphous carbon films by incorporation of nitrogen," *Thin Solid Films*, vol. 353, iss. 1-2, pp. 157-165, Sep. 1999, doi: 10.1016/S0040-6090(99)00421-6.

[30] S. Zhang, H. Du, S. E. Ong, K. N. Aung, H. C. Too, and X. Miao, "Bonding structure and hemocompatibility of silicon-incorporated amorphous carbon," *Thin Solid Films*, vol. 515, iss. 1, pp. 66-72, Sep. 2006, doi: 10.1016/j.tsf.2005.12.037.

[31] C. C. Chen and F. C. N. Hong, "Structure and properties of diamond-like carbon nanocomposite films containing copper nanoparticles," *Applied Surface Science*, vol. 242, iss. 3-4, pp. 261-269, doi: 10.1016/j.apsusc.2004.08.036.

[32] J. Robertson and C. A. Davis, "Nitrogen doping of tetrahedral amorphous carbon," *Diamond and Related Materials*, vol. 4, iss. 4, pp. 441-444, Apr. 1995, doi: 10.1016/0925-9635(94)05265-4.

[33] R. Garg, S. Gonuguntla, S. Sk, M. S. Iqbal, A. O. Dada, U. Pal, and M. Ahmadipour, "Sputtering thin films: materials, applications, challenges, and future directions," *Advances in Colloid and Interface Science*, vol. 330, pp. 103203, Aug. 2024, doi: 10.1016/j.cis.2024.103203.

[34] C. S. Lee, T. Y. Kim, K. R. Lee, and K. H. Yoon, "Nanoscale manipulation of tetrahedral amorphous carbon films," Thin Solid Films, vol. 447-448, pp. 169-173, Jan. 2004, doi: 10.1016/S0040-6090(03)01075-7.

[35] A. Oya and S. Otani, "Catalytic graphitization of carbons by various metals," *Carbon*, vol. 17, iss. 2, pp. 131-137, 1979, doi: 10.1016/0008-6223(79)90020-4.

[36] D. Bootkul, B. Supsermpol, N. Saenphinit, C. Aramwit, and S. Intarasiri, "Nitrogen doping for adhesion improvement of DLC film deposited on Si substrate by filtered cathodic vacuum arc technique," *Applied Surface Science*, vol. 310, pp. 284-292, Aug. 2014, doi: 10.1016/j.apsusc.2014.03.059.

[37] J. Zemek, J. Houdkova, P. Jiricek, and T. Kocourek, "Amorphous carbon nitride films: surface and subsurface composition and bonding," *Langmuir*, vol. 40, iss. 37, pp. 19538-19547, Aug. 2024, doi: 10.1021/acs.langmuir.4c02007.

[38] N. K. Manninen, F. Ribeiro, A. Esudeiro, T. Polcar, S. Carvalho, and A. Cavaleiro, "Influence of Ag content on mechanical and tribological behavior of DLC coatings," *Surface and Coatings Technology*, vol. 232, pp. 440-446, Oct. 2013, doi: 10.1016/j.surfcoat.2013.05.048.

[39] J. Zemek, J. Houdkova, P. Jiricek, and M. Jelinek, "Surface and in-depth distribution of sp^2 and sp^3 coordinated carbon atoms in diamond-like carbon films modified by argon ion beam bombardment during growth," *Carbon*, vol. 134, pp. 71-79, Aug. 2018, doi: 10.1016/j.carbon.2018.03.072.

[40] C. T. Kuo, C. R. Lin, and H. M. Lien, "Origins of the residual stress in CVD diamond films," *Thin Solid Films*, vol. 290-291, pp. 254-259, Dec. 1996, doi: 10.1016/S0040-6090(96)09016-5.

[41] J. C. Augus and F. Jansen, "Dense diamond-like hydrocarbons as random covalent networks," *Journal of Vacuum Science and Technology A*, vol. 6, iss. 3, pp. 1778-1782, May 1988, doi: 10.1116/1.575296.

[42] J. P. Sullivan, T. A. Friedmann, and A. G. Baca, "Stress relaxation and thermal evolution of film properties in amorphous carbon," *Journal of Electronic Materials*, vol. 26, pp. 1021-1029, Sep. 1997, doi: 10.1007/s11664-997-0239-9.

[43] N. Kametani, M. Nakamura, K. Yashiro, and T. Takaki, "Investigating residual stress evolution in the deposition process of diamond-like carbon film through molecular dynamics," *Computational Materials Science*, vol. 209, pp. 111420, Jun. 2022, doi: 10.1016/j.commatsci.2022.111420.

[44] N. W. Khun and E. Liu, "Enhancement of adhesion strength and corrosion resistance of nitrogen or platinum/ruthenium/nitrogen-doped diamond-like carbon thin films by platinum/ruthenium underlayer," *Diamond and Related Materials*, vol. 19, iss. 7-9, pp. 1065-1072, Sep. 2010, doi: 10.1016/j.diamond.2010.03.009.

[45] J. S. Wang and A. G. Evans, "Measurement and analysis of buckling and buckle propagation in compressed oxide layers on superalloy substrates," *Acta Materialia*, vol. 46, iss. 14, pp. 4993-5005, Sep. 1998, doi: 10.1016/S1359-6454(98)00172-4.

[46] M. W. Moon, J. W. Chung, K. R. Lee, K. H. Oh, R. Wang, and A. G. Evans, "An experimental study of the influence of imperfections on the buckling of compressed thin films," *Acta Materialia*, vol. 50, iss. 4, pp. 1219-1227, Mar. 2002, doi: 10.1016/S1359-6454(01)00423-2.

[47] D. Sheeja, B. K. Tay, K. W. Leong, and C. H. Lee, "Effect of film thickness on the stress and adhesion of diamond-like carbon coatings," *Diamond and Related Materials*, vol. 11, iss. 9, pp. 1643-1647, Sep. 2002, doi: 10.1016/S0925-9635(02)00109-7.

[48] L. Liu, Z. Wu, X. An, S. Xiao, S. Cui, H. Lin, R. K. Y. Fu, X. Tian, R. Wei, P. K. Chu, and F. Pan, "Excellent adhered thick diamond-like carbon coatings by optimizing hetero-interfaces with sequential highly energetic Cr and C ion treatment," *Journal of Alloys and Compounds*, vol. 735, pp. 155-162, Feb. 2018, doi: 10.1016/j.jallcom.2017.11.057.

[49] H. He and M. F. Thorpe, "Elastic properties of glasses," Physical Review Letters, vol. 54, iss. 19, pp. 2107, May 1985, doi: 10.1103/PhysRevLett.54.2107.

[50] L. Ji, Y. Wu, H. Li, H. Song, X. Liu, Y. Ye, J. Chen, H. Zhou, and L. Liu, "The role of trace Ti concentration on the evolution of microstructure and properties of duplex-doped Ti(Ag)/DLC films," *Vacuum*, vol. 115, pp. 23-30, May 2015, doi: 10.1016/j.vacuum.2015.01.023.

[51] N. Boubiche, J. E. Hamouchi, J. Hulik, M. Abdesslam, C. Speisser, F. Djeffal, and F. L. Normand, "Kinetics of graphitization of thin diamond-like carbon films catalyzed by transitional metal," *Diamond and Related Materials*, vol. 91, pp. 190-198, Jan. 2019, doi: 10.1016/j.diamond.2018.10.025.

[52] P. C. Tsai, Y. F. Hwang, J. Y. Chaiang, and W. J. Chen, "The effects of deposition parameters on the structure and properties of titanium-containing DLC films synthesized by cathodic arc plasma evaporation," *Surface and Coatings Technology*, vol. 202, iss. 22-23, pp. 5350-5355, Aug. 2008, doi: 10.1016/j.surfcoat.2008.06.073.

[53] S. Logothetidis, M. Gioti, P. Patsalas, and C. Charitidis, "Insights on the deposition mechanism of sputtered amorphous carbon films," *Carbon*, vol. 37, iss. 5, pp. 765-769, Apr. 1999, doi: 10.1016/S0008-6223(98)00268-1.

[54] M. M. M. Bilek and D. R. McKenzie, "A comprehensive model of stress generation and relife processes in thin films deposited with energetic ions," *Surface and Coatings Technology*, vol. 200, iss. 14-15, pp. 4345-4354, Apr. 2006, doi: 10.1016/j.surfcoat.2005.02.161.

[55] L. Wang, L. Li, and X. Kuang, "Effect of substrate bias on microstructure and mechanical properties of WC-DLC coatings deposited by HiPIMS," *Surface and Coatings Technology*, vol. 352, pp. 33-41, Oct. 2018, doi: 10.1016/j.surfcoat.2018.07.088.

[56] C. D. Dieleman, P. J. Denissen, and S. J. Garcia, "Long-term active corrosion protection of damaged coated AA2024-T3 by embedded electrospun inhibiting nanonetworks," *Advanced Materials Interfaces*, vol. 5, iss. 12, pp. 1800176, Jun. 2018, doi: 10.1002/admi.201800176.

[57] K. B. Oldham, "The RC time "constant" at a disk electrode," *Electrochemistry Communications*, vol. 6, iss. 2, pp. 210-214, Feb. 2004, doi: 10.1016/j.elecom.2003.12.002.

[58] S. R. P. Silva, J. Robertson, G. A. J. Amaratunga, B. Rafferty, J. Schwan, D. F. Franceschini, and G. Mariotto, "Nitrogen modification of hydrogenated amorphous carbon films," *Journal of Applied Physics,* vol. 81, pp. 2626-2634, Mar. 1977, doi: 10.1063/1.363927.

[59] L. Wang, C. Feng, H. Liu, D. Yi, L. Jiang, and Y. Feng, "Revealing the role of Ru in improving corrosion resistance of titanium alloys in HCl solution, *Heat Treatment and Surface Engineering*, vol. 1, iss. 3-4, pp. 97-108, Oct. 2019, doi: 10.1080/25787616.2020.1743038.

[60] K. I. Schiffmann, M. Fryda, G. Goerigk, R. Lauer, P. Hinze, and A. Bulack, "Sizes and distance of metal clusters in Au, Pt, W and Fe-containing diamond-like carbon hard coatings: a comprehensive study by small-angle X-ray scattering, wide angle X-ray diffraction, transmission electronmicroscopy and scanning tunneling microscopy," *Thin Solid Films*, vol. 347, iss. 102, pp. 60-71, Jun. 1999, doi: 10.1016/S0040-6090(98)01607-1.

[61] Y. V. Pleskov, Y. E. Evstefeeva, and A. M. Baranov, "Threshold effect of admixtures of platinum on the electrochemical activity of amorphous diamond-like carbon thin films," *Diamond and Related Materials*, vol. 11, iss. 8, pp. 1518-1522, Aug. 2002, doi: 10.1016/S0925-9635(02)00057-2.

[62] W. Peng, H. Luo, and J. Tang, "Electron transfer kinetics and corrosion resistance of electrodeposited composite coating on titanium alloy," *Corrosion Science*, vol. 176, pp. 108918, Nov. 2020, doi: 10.1016/j.corsci.2020.108918.

[63] N. W. Khun and E. Liu, "Effect of platinum and ruthenium incorporation on voltammetric behaviour of nitrogen-doped diamond-like carbon thin films," *Electroanalysis*, vol. 21, iss. 23, pp. 2590-2596, Dec. 2009, doi: 10.1002/elan.200900250.